Effects of multiple ionization and intrashell coupling in *L*-subshell ionization by heavy ions

Gregory Lapicki,[1,*] G. A. V. Ramana Murty,[2] G. J. Naga Raju,[2] B. Seetharami Reddy,[2] S. Bhuloka Reddy,[2] and V. Vijayan[3]
[1]*Department of Physics, East Carolina University, Greenville, North Carolina 27858, USA*
[2]*Swami Jnanananda Laboratories for Nuclear Reasearch, Andhra University, Visakhapatnam-530 003, India*
[3]*Institute of Physics, Sachivalaya Marg, Bhubaneswar-751 005, India*
(Received 9 February 2004; published 28 December 2004)

L-subshell ionization cross sections are extracted from measured $L\alpha$, $L\beta$, $L\gamma$, $L\gamma_1$, $L\gamma_{23}$, and $L\gamma_{44}$ x-ray production cross sections in thin targets of $_{75}$Re, $_{78}$Pt, and $_{79}$Au bombarded by 4–8 MeV C^{3+} ions. For each projectile energy, using the fluorescence and Coster-Kronig yields recently recommended by Campbell with an amendment for multiple ionization effects, a mutually consistent set of ionization cross sections is extracted from $L\alpha$ and six pairs of other *L*-line x-ray production cross sections. Extracted L_1-, L_2-, L_3-ionization cross sections are compared with the predictions of the ECPSSR theory—which accounts for the energy (E) loss and Coulomb (C) deflection of the projectile as well as for perturbed-stationary state (PSS) and relativistic (R) nature of *L* subshells—and its modification, ECUSAR-IS. In the ECUSAR-IS theory, the PSS effect is calculated with a united and separated atom (USA) treatment and the intrashell (IS) coupling is accounted for by multiplicative factors of Sarkadi and Mukoyama normalized so that the sum of *L*-subshell ECUSAR-IS cross sections equals ECUSAR *L*-shell ionization cross section without the IS correction. Further improvement of this theory to account for better wave functions in its evaluation is made by scaling it with ratios of Dirac-Hartree-Slater cross sections to the screened hydrogenic formulas used in the ECPSSR theory. Very good agreement is obtained with L_2 and L_3 ionization data. For the L_1 subshell, the data are in good agreement with the ECPSSR theory but are by factors of 2 to 3 above the results of its modifications.

DOI: 10.1103/PhysRevA.70.062718 PACS number(s): 34.50.Fa

I. INTRODUCTION

The literature abounds with *K*- and *L*-shell ionization cross sections by protons and α particles. Compilations of these data [1–5] show generally good (i.e., within the claimed experimental uncertainties) agreement of *K*- and total *L*-shell ionization data with the ECPSSR theory that goes beyond the first Born approach [6,7] by accounting for the energy loss (E) and Coulomb-deflection (C) of the projectile, and for perturbed-stationary state (PSS) and relativistic (R) nature of the target both for direct ionization [8] and electron capture [9]. However, even with protons, there are systematic deviations in the prediction of *L*-subshell ionization cross sections [5,10].

Less frequent measurements of *L*-subshell cross sections induced by heavy ions further expose these deviations. In part, such deviations are traced to methods of extraction of ionization cross sections from x-ray production measurements. These methods can result in inconsistent results because fluorescence yields and other parameters required for extraction of *L*-subshell ionization cross sections are strongly affected by the prevalence of multiple ionization by heavy ions. Section II describes the experimental setup, presents data analysis to obtain cross sections for x-ray production in $_{75}$Re, $_{78}$Pt, and $_{79}$Au bombarded by C^{3+} ions, discusses extraction of L_1-, L_2-, L_3-ionization cross sections from these data, and lists the present data as well the data found in the literature for ionization of these targets by carbon ions.

The extracted *L*-subshell ionization cross sections are compared in Sec. III with the predictions of the first Born approximation [6,7], the ECPSSR theory [8,9] and its modifications with a united and separated atom (USA) approach and normalized intrashell (IS) coupling factors. Results of our methods of accounting for multiple ionization are contrasted with those of Pajek *et al.* [11]. The role of better wave functions in evaluation of ECPSSR formulas is discussed in Sec. IV. Section V summarizes our findings and points to a possible culprit behind the persistent discrepancies in the L_1 ionization cross sections.

II. EXTRACTION OF X-RAY PRODUCTION AND *L*-SUBSHELL IONIZATION CROSS SECTIONS

The present experiment was performed using a 3 MV pelletron accelerator at the Institute of Physics in Bhubaneswar. Thin foils of Re (15 μg/cm^2), Pt (12 μg/cm^2), and Au (8 μg/cm^2) were prepared by vacuum evaporation, and positioned in the scattering chamber at an angle of 45° with respect to the C^{3+} ion beam. With respect to that beam, a Si(Li) detector (with a 160 eV FWHM resolution at 5.9 keV) recorded *L*-x-ray spectra at 90° and a surface barrier detector detected the backscattered particles at 135°. The spectra were gathered for sufficiently long time to obtain good statistics. A typical *L* x-ray spectrum from 8-MeV carbon impinging on gold is shown in Fig. 1.

From the measured yield in an Lp peak ($p=\alpha,\beta,\gamma,\ldots$) of the x-ray spectrum, Y_{Lp}, and the measured scattered particle yield, Y_P, the Lp x-ray production cross section obtains as

*Electronic address: lapicki@physicist.net

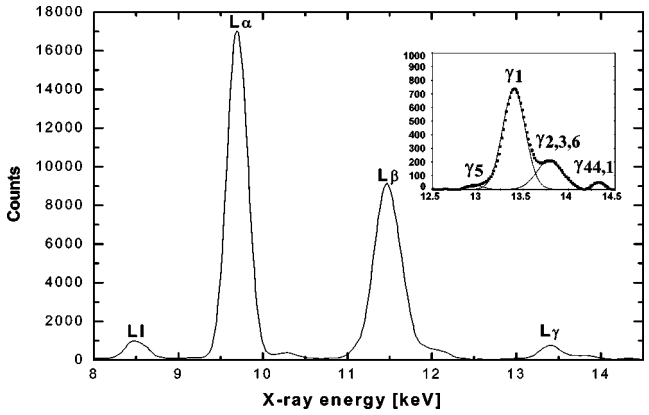

FIG. 1. *L* x-ray spectrum of gold bombarded by 8-MeV C^{3+} ions.

$$\sigma_{Lp} = 4\pi Y_{Lp}\sigma_R(\theta)\Delta\Omega_P t_X/t_P \varepsilon Y_P \Delta\Omega_X s, \tag{1}$$

where $\sigma_R(\theta)$ is the Rutherford differential cross section, $\Delta\Omega_P$ and $\Delta\Omega_X$ are the solid angles subtended by the charged particle and x-ray detectors, t_P and t_X are their dead time corrections, ε is the efficiency of the Si(Li) x-ray detector, and $s=(1-e^{-\mu x})/\mu x$ is the self-absorption correction in a target foil of thickness x. The efficiency curve of the Si(Li) detector was calculated from the detector specifications supplied by its manufacturer, and verified with standard radioactive sources.

Table I lists the measured x-ray production cross sections. From these measurements and the data of others for gold [12–15] and platinum [15], *L*-subshell ionization cross sections, σ_{Li} $(i=1,2,3)$, will be extracted for comparison with predictions of the ECPSSR theory and its modifications. In terms of σ_{Li}, the x-ray production cross sections can be calculated as follows:

TABLE I. Measured *L* x-ray production cross sections (b) for C^{3+} on rhenium, platinum, and gold.

E_1 (MeV)	$L1$	$L\alpha$	$L\beta$	$L\gamma$	$L\gamma_1$	$L\gamma_{23}$	$L\gamma_{44}$
$_{75}$Re							
4	0.15	3.06	2.81	0.472	0.255	0.180	0.0287
5	0.38	7.20	6.27	1.03	0.646	0.322	0.0518
6	0.76	13.3	10.3	1.63	0.992	0.516	0.0826
7	1.22	23.6	16.7	2.54	1.60	0.630	0.0980
8	1.60	31.3	22.4	3.40	2.25	0.945	0.154
$_{78}$Pt							
4	0.20	2.27	1.88	0.317	0.199	0.104	0.0147
5	0.29	5.26	4.13	0.659	0.415	0.173	0.0302
6	0.47	9.01	6.71	1.07	0.672	0.264	0.0459
7	0.80	15.9	10.8	1.66	1.13	0.422	0.0733
8	1.17	22.5	14.4	2.13	1.44	0.506	0.0880
$_{79}$Au							
4	0.16	2.05	1.91	0.340	0.187	0.114	0.0210
5	0.28	3.79	2.61	0.412	0.261	0.150	0.0275
6	0.43	7.65	5.13	0.798	0.471	0.254	0.0466
7	0.68	13.8	8.16	1.18	0.781	0.331	0.0615
8	1.13	20.3	12.2	1.78	1.25	0.468	0.0873

TABLE II. Atomic parameters for single-vacancy atoms: fluorescence and Coster-Kronig yields [17], and fractional radiative transitions $S_{pi}=\Gamma_p/\Gamma_i$ based on [16].

	$_{75}$Re	$_{78}$Pt	$_{79}$Au
ω_1^o	0.15	0.13	0.13
ω_2^o	0.304	0.344	0.358
$\omega^o{}_3$	0.271	0.303	0.313
f_{12}^o	0.07	0.07	0.07
f_{13}^o	0.32	0.56	0.58
f_{23}^o	0.131	0.126	0.125
$S\alpha_3$	0.793	0.782	0.779
$S\beta_1$	0.753	0.744	0.741
$S\beta_2$	0.801	0.792	0.789
$S\beta_3$	0.168	0.178	0.181
$S\gamma_1$	0.226	0.231	0.233
$S\gamma_2$	0.177	0.185	0.189
$S\gamma_{1,2}$	0.160	0.164	0.165
$S\gamma_{23,1}$	0.192	0.194	0.194
$S\gamma_{44',1}$	0.0308	0.0335	0.0345

$$\sigma_{L\alpha} = [\sigma_{L_1}(f_{12}f_{23}+f_{13}) + \sigma_{L_2}f_{23} + \sigma_{L_3}]\omega_3 S_{\alpha_3}, \tag{2}$$

$$\sigma_{L\beta} = \sigma_{L_1}[\omega_1 S_{\beta_1} + f_{12}\omega_2 S_{\beta_2} + (f_{12}f_{23}+f_{13})\omega_3 S_{\beta_3}] + \sigma_{L_2}(\omega_2 S_{\beta_2} + f_{23}\omega_3 S_{\beta_3}) + \sigma_{L_3}\omega_3 S_{\beta_3}, \tag{3}$$

$$\sigma_{L\gamma} = \sigma_{L_1}(\omega_1 S_{\gamma_1} + f_{12}\omega_2 S_{\gamma_2}) + \sigma_{L_2}\omega_2 S_{\gamma_2}, \tag{4}$$

$$\sigma_{L\gamma_1} = (\sigma_{L_1}f_{12} + \sigma_{L_2})\omega_2 S_{\gamma_{1,2}}, \tag{5}$$

$$\sigma_{L\gamma_{23}} = \sigma_{L_1}\omega_1 S_{\gamma_{23,1}}, \tag{6}$$

$$\sigma_{L\gamma_{44'}} = \sigma_{L_1}\omega_1 S_{\gamma_{44',1}}. \tag{7}$$

The target atomic parameters in the above set of equations are: the fluorescence yields ω_i, the Coster-Kronig yields f_{ij}, and $S_{pi}=\Gamma_p/\Gamma_i$ that is the fraction of the radiative transition to the *i*th subshell associated with the L_p peak. These fractions were evaluated with Γ's taken from Campbell and Wang [16]; for the fluorescence and Coster-Kronig yields we start with the single-vacancy, ω_j^o and f_{ij}^o, values recently recommended by Campbell [17]. These values are listed in Table II as an initial set of atomic parameters—without consideration of multiple ionization and intrashell coupling effects.

It has been known for over three decades that simultaneous ionization of *L* and higher subshells affects *L*-subshell ionization; increasingly so when heavier projectile ions are used [18]. Originally, the number of additional vacancies in higher subshells was deduced from the measured x-ray en-

ergy shifts [18,19]. In the energy range that overlaps with our present work for C→Pt and Au, following Berinde *et al.* [20], Semaniak *et al.* [15] derived the probabilities for ionization of *M* and *N* subshells from changes in relative *L* x-ray peak yields once protons were replaced with carbon ions. While, with Larkins scaling [21] to deduce the number of multiple vacancies from energy shifts and relative intensities redistribution, this approach evolved into a standard procedure [22], Pajek *et al.* [23] demonstrated that changes in both position and width of x-ray peaks are the most reliable determinants of the outer-shell ionization probabilities. Pajek *et al.* [23] combined the energy shifts and the widths broadening as an experimental input to extract these probabilities and showed them to be in a fair agreement with a binary encounter approximation geometrical model of Sulik *et al.* [24].

Since we have not measured these shifts and broadenings, we corrected the single-hole fluorescence and CK yields of Campbell [17], ω_i^o and f_{ij}^o, using a simplified assumption that each electron in a manifold of outer subshells is ionized with a probability *P*. With all radiative transition widths narrowed by the same factor, 1-*P*, and with all Auger rates—involving two electrons in the manifold of outer states as well as the Coster-Kronig transitions—decreased by $(1\text{-}P)^2$, Lapicki *et al.* [25] obtained ω_i corrected for simultaneous ionization in outer subshells

$$\omega_i = \omega_i^o/[1 - P(1 - \omega_i^o)], \tag{8}$$

while f_{ij}^o is reduced to

$$f_{ij} = f_{ij}^o(1 - P)^2. \tag{9}$$

After, as stated in Ref. [26], replacement of the projectile atomic number Z_1 with its charge state *q*, the probability *P* of ionizing an outer shell electron is calculated according to Eq. (A3) of Ref. [25]:

$$P = q^2(1 - \beta/4v_1^2)/2\beta v_1^2, \tag{10}$$

where $\beta = 0.9$ and $v_1 = 6.351\ [E_1(\mathrm{MeV})/A_1(\mathrm{u})]^{1/2}$ is the projectile velocity. For charge state *q*, we take the incident charge for thin (such as our $8-15\ \mu\mathrm{g/cm^2}$) targets or the mean equilibrium charge [27] for targets that are sufficiently thick—as was the Au target of Ref. [13]—for *q* to settle into its equilibrium state. Tables III and IV show multiple ionization factors MI, defined as the ratio of *L*-subshell ionization cross section extracted without any multiple ionization correction to the ones that were extracted with the multiple ionization accounted for as given by Eqs. (8)–(10).

Following ionization, electrons in ionized atoms cascade along a variety of pathways depending strongly on the primary patterns of multiple ionization of an inner shell and outer shells [28]. L_1 deexcitation in free atoms leads to the higher ionization stages than in the aftermath of vacancy creation in L_2 and L_3 [29]. For solid targets of our experiment, this finding may not hold since combined effects of multiple scattering and dynamical screening in ion-solid collisions enhance the population of $2p$ states [30]. Discussing differences in x-ray production in solid and gaseous targets by heavy ions, Lutz *et al.* [31] noted that in a solid all vacancies above the *M* shell are probably filled. This would make the production of an x-ray more likely than of an Auger electron. In particular, the $L\gamma_{23}$ and $L\gamma_{44}$ x-ray cross sections would be most enhanced since they involve the outermost shells most probably to be filled by electrons in solids; increased solid-state values of ω_1 would yield through Eqs. (6) and (7) smaller ionization cross sections for the L_1 subshell. Yet, Lutz *et al.* [31] also argued that the milieu of high electron density in a solid may tend to enhance decay via less selective nonradiative transitions and, thus, cause an effective suppression of the fluorescence yield. The contradictory and uncertain outcome of such arguments for deexcitation of ionized atoms in solids is not much less certain in analysis of electron cascades in free atoms where the results are obscured by uncertain contributions of different subshells and the lack of the self consistency in the selected database for x-ray, nonradiative, and electron shake-off rates [29]. Depending rather sensitively on these uncertainties, channels for super Coster-Kronig transitions may very well be opened or energetically forbidden for some CK transitions; particularly so when multiple ionizations enlarge number of ways in which electrons can cascade and, in a complex feedback fashion, modify the rates of these transitions. As demonstrated by Sorensen *et al.* [32], the question of whether a CK transition is closed in a free atom and open in a metallic target of the same element can be answered with the technique of the selective subshell ionization by tuned synchrotron radiation. For a particular primary vacancy distribution in a sample of multiply-ionized atoms created in a given collision with a gaseous or solid target, however, one would have to use synchrotron radiation *in situ* to decide unambiguously which CK transitions are energetically available. An analysis of the effects of an *L*-shell spectator vacancy on *L* x-ray emission by Lorenz and Hartmann [33] indicates that the average changes in the fluorescence yield are more reliable than the nuances of transition probabilities for particular cascade schemes. It is the spirit of this finding that supports our simplified assumption that each electron in a manifold of outer subshells is ionized with same probability in Eqs. (8) and (9).

L_1, L_2, and L_3 ionization cross sections could be derived from any subset of three equations from Eqs. (2)–(7). With the $L\alpha$ peak containing about $\frac{1}{2}$ of all x rays in the spectrum, Eq. (2) is an indispensable component in every subset of Eqs. (2)–(7). In conjunction with this peak, 4 pairs—$\{L\beta, L\gamma\}$, $\{L\gamma_1, L\gamma_{44}\}$, $\{L\gamma, L\gamma_1\}$, and $\{L\gamma_1, L\gamma_{23}\}$—are commonly employed in the extraction of *L*-subshell ionization cross sections as they were discussed two decades ago by Cohen [34] and, more recently, by Singh *et al.* [35]. We have extracted the ionization cross sections by 3 additional methods: using the two most prominent peaks, $L\alpha$ and $L\beta$, in combination with $L\gamma_1$, $L\gamma_{23}$, or $L\gamma_{44}$. In the methods that require $L\gamma_{23}$ cross section, $L\gamma_{23}$ was derived from $L\gamma_{23,6}$ and $L\gamma_6$ peaks by the Datz technique [36] which, as found by Cohen [37], is most critical for ion energies around 1 MeV/u and for heavy targets. The first method—based on 3 major peaks $L\alpha$, $L\beta$, and $L\gamma$—is the most reliable statistically because it is grounded on the largest and well separated peaks in the x-ray spectrum. However, as noted by Jitschin *et al.* [38] "the contributions from L_1 and L_2 to $L\beta$ and $L\gamma$ are

TABLE III. *L*-subshell ionization cross sections (b) for 4–8 MeV C^{+3} on Re, Pt, and Au extracted from the measured x-ray production cross sections using radiative rates of Campbell and Wang [16] and fluorescence yields of Campbell [17], corrected for the multiple ionization according to Eqs. (8)–(10). The listed cross sections, which are the mean of the values obtained from $L\alpha$ and six pairs of the other two x-ray peaks, are followed with the ratios of these values to listed mean cross sections; the $L\beta L\gamma$ pair was not used in calculation of the mean. Also shown are the multiple ionization (MI) factors calculated as the ratios of ionization cross sections extracted without-to-with correction of the fluorescence yields for the MI effect.

		4 MeV			5 MeV			6 MeV			7 MeV			8 MeV		
		L_1	L_2	L_3	L_1	L_2	L_3	L_1	L_2	L_3	L_1	L_2	L_3	L_1	L_2	L_3
$_{75}$Re		**4.48**	**3.97**	**9.65**	**8.62**	**10.5**	**24.2**	**14.6**	**16.9**	**46.9**	**18.0**	**30.5**	**86.8**	**28.5**	**39.9**	**116**
$L\alpha$	$L\beta L\gamma$	0.30	1.49	1.03	0.31	1.34	1.03	0.10	1.46	1.04	0.07	1.32	1.03	0.15	1.36	1.03
$L\alpha$	$L\gamma_1 L\gamma_{44}$	0.95	0.95	1.00	0.98	0.98	1.00	0.97	0.97	1.00	0.97	0.98	1.00	0.99	0.98	1.00
$L\alpha$	$L\gamma L\gamma_1$	0.97	0.95	1.00	0.94	0.98	1.00	0.92	0.97	1.01	0.89	0.98	1.01	0.91	0.98	1.01
$L\alpha$	$L\gamma_1 L\gamma_{23}$	0.96	0.95	1.00	0.97	0.98	1.00	0.97	0.97	1.00	1.00	0.98	1.00	0.97	0.98	1.00
$L\alpha$	$L\beta L\gamma_1$	1.20	0.95	0.99	1.16	0.97	0.99	1.21	0.96	0.99	1.18	0.98	0.99	1.18	0.97	0.99
$L\alpha$	$L\beta L\gamma_{23}$	0.96	1.09	1.00	0.97	1.05	1.00	0.97	1.07	1.00	1.00	1.03	1.00	0.97	1.05	1.00
$L\alpha$	$L\beta L\gamma_{44}$	0.95	1.10	1.00	0.98	1.05	1.00	0.97	1.07	1.00	0.97	1.04	1.00	0.99	1.04	1.00
MI	factor	1.45	1.27	1.19	1.33	1.22	1.16	1.26	1.17	1.14	1.22	1.15	1.13	1.19	1.13	1.11
$_{78}$Pt		**2.60**	**2.64**	**6.41**	**5.49**	**6.00**	**15.7**	**8.74**	**10.0**	**28.0**	**13.7**	**16.8**	**51.1**	**17.3**	**22.0**	**74.4**
$L\alpha$	$L\beta L\gamma$	0.62	1.18	1.03	−0.1	1.48	1.09	−0.3	1.55	1.12	0.58	1.16	1.04	0.15	1.31	1.07
$L\alpha$	$L\gamma_1 L\gamma_{44}$	0.89	0.99	1.04	0.94	0.96	1.01	0.95	0.96	1.01	1.00	0.99	1.00	0.98	0.98	1.00
$L\alpha$	$L\gamma L\gamma_1$	0.97	0.99	1.00	0.96	0.96	1.00	0.90	0.96	1.01	0.94	1.00	1.01	0.2	0.98	1.01
$L\alpha$	$L\gamma_1 L\gamma_{23}$	1.08	0.98	0.99	0.93	0.96	1.01	0.94	0.96	1.01	1.00	0.99	1.00	0.98	0.98	1.00
$L\alpha$	$L\beta L\gamma_1$	1.09	0.98	0.99	1.30	0.95	0.97	1.32	0.95	0.97	1.06	0.99	0.99	1.17	0.98	0.99
$L\alpha$	$L\beta L\gamma_{23}$	1.08	0.99	0.99	0.93	1.09	1.00	0.94	1.08	1.00	1.00	1.01	1.00	0.98	1.04	1.00
$L\alpha$	$L\beta L\gamma_{44}$	0.89	1.07	1.00	0.94	1.09	1.00	0.95	1.08	1.00	1.00	1.01	1.00	0.98	1.04	1.00
MI	factor	1.47	1.25	1.09	1.34	1.19	1.09	1.27	1.16	1.08	1.22	1.13	1.08	1.19	1.11	1.08
$_{79}$Au		**3.26**	**2.42**	**5.41**	**4.39**	**3.34**	**10.9**	**8.22**	**6.50**	**22.9**	**10.9**	**10.9**	**43.6**	**15.5**	**17.6**	**65.2**
$L\alpha$	$L\beta L\gamma$	0.34	1.42	1.09	1.71	0.57	0.92	0.68	1.19	1.04	1.18	0.92	0.99	1.70	0.72	0.94
$L\alpha$	$L\gamma L\gamma_{44}$	0.98	0.96	1.00	1.04	1.03	0.99	0.99	0.98	1.00	1.03	1.01	1.00	1.05	1.02	0.99
$L\alpha$	$L\gamma L\gamma_1$	0.97	0.97	1.00	1.05	1.03	0.99	0.99	0.98	1.00	1.01	1.01	1.00	1.05	1.02	1.00
$L\alpha$	$L\gamma_1 L\gamma_{23}$	0.95	0.97	1.01	1.01	1.03	1.00	0.96	0.98	1.00	0.99	1.01	1.00	1.00	1.02	1.00
$L\alpha$	$L\beta L\gamma_1$	1.17	0.96	0.98	0.85	1.04	1.02	1.09	0.98	0.99	0.95	1.01	1.00	0.84	1.03	1.01
$L\alpha$	$L\beta L\gamma_{23}$	0.95	1.08	1.00	1.01	0.95	1.00	0.96	1.04	1.00	0.99	0.99	1.00	1.00	0.97	1.00
$L\alpha$	$L\beta L\gamma_{44}$	0.98	1.06	1.00	1.04	0.93	1.00	0.99	1.03	1.00	1.03	0.98	1.00	1.05	0.95	1.00
MI	factor	1.47	1.22	0.97	1.34	1.17	1.06	1.27	1.13	1.06	1.22	1.12	1.08	1.19	1.11	1.07

comparable" and therefore "the L_1 and L_2 cross sections obtained by this procedure are rather sensitive to the accurate $L\beta$ and $L\gamma$ intensities as well as the branching ratios of the L_1 and L_2 subshells." Furthermore, Eqs. (2)–(4) require the greatest number of atomic parameters. Hence, in Table III we report the measured *L*-subshell ionization cross sections as an arithmetic average of the values obtained with 6 other combinations of three peaks from the measured x-ray spectrum. Indeed the first method as listed in this table was not included in our average because it yielded cross sections at a great variance from the means obtained from the remaining six methods. As shown in Table III, the ratios of cross sections extracted by any one of these six methods to their means gravitate around 1; mostly within a few percent of 1 and with no deviation above 32%. Given 10–20 % experimental uncertainties in deriving x-ray production cross sections from the measured x-ray spectra by Eq. (1), such deviations are well within the norm of what one might expect in the normal distribution of errors for 270 ratios displayed in Table III. This consistency could be viewed as means of validation of the data and their analysis. An ill-defined inverse matrix that transforms the input x-ray peak cross sections to the ionization cross sections could indicate that a choice of atomic parameters with their corrections for mul-

TABLE IV. *L*-subshell ionization cross sections (b) for C^{q+} on Au from Refs. [12–14], corrected for the multiple ionization according to Eqs. (8)–(10). The multiple ionization factors listed below the cross sections were calculated as the ratios of ionization cross sections extracted without-to-with correction of the gold for the MI effect. This table does not show the data from Semaniak *et al.* [15] because their *L*-subshell ionization cross sections were already corrected for multiple ionization effects.

L_1	L_2	L_3	L_1	L_2	L_3	L_1	L_2	L_3	L_1	L_2	L_3
Sarkadi and Mukoyama (1980)			$q=1$								Ref. [12]
2.5 MeV			2.8 MeV			3.1 MeV			3.4 MeV		
0.108	**0.155**	**0.140**	**0.240**	**0.301**	**0.235**	**0.445**	**0.553**	**0.484**	**0.857**	**1.04**	**1.00**
1.06	1.04	0.96	1.05	1.03	0.95	1.05	1.03	0.96	1.04	1.03	0.97
Malhi and Gray (1991)						q=equilibrium charge (Ref. [27])					Ref. [13]
7.0 MeV			9.5 MeV			10.7 MeV			11.9 MeV		
8.35	**13.2**	**31.2**	**19.4**	**31.7**	**87.9**	**33.3**	**51.7**	**138**	**42.8**	**71.0**	**198**
1.61	1.34	1.20	1.47	1.27	1.18	1.43	1.24	1.16	1.39	1.23	1.15
14.3 MeV			15.5 MeV			16.7 MeV			17.9 MeV		
59.5	**94.5**	**278**	**75.6**	**123**	**365**	**79.8**	**139**	**447**	**93.3**	**156**	**489**
1.33	1.20	1.13	1.31	1.18	1.13	1.29	1.17	1.13	1.27	1.16	1.12
20.3 MeV			21.5 MeV			23 MeV			25 MeV		
121	**200**	**646**	**148**	**234**	**770**	**169**	**264**	**853**	**211**	**334**	**1140**
1.25	1.15	1.11	1.23	1.14	1.10	1.22	1.13	1.09	1.20	1.12	1.09
28 MeV			30 MeV			32 MeV			36 MeV		
295	**439**	**1520**	**402**	**557**	**1910**	**587**	**773**	**2680**	**824**	**987**	**3370**
1.18	1.11	1.08	1.17	1.10	1.07	1.16	1.09	1.06	1.15	1.08	1.05
Bhattacharya *et al.* (1994)						$q=2$ at 3.6 MeV and $q=3$ at 4.8–9.5 MeV					Ref. [14]
3.6 MeV			4.8 MeV			7.2 MeV			9.5 MeV		
0.575	**0.895**	**1.48**	**2.00**	**3.02**	**6.87**	**4.75**	**10.5**	**29.9**	**10.6**	**21.1**	**71.0**
1.19	1.11	1.02	1.36	1.21	1.10	1.22	1.14	1.10	1.16	1.10	1.08

tiple ionization is inapplicable in Eqs. (2)–(7). The fact that we have not encountered such ill-defined matrices in any of the 6 methods does not guarantee that our choice of radiative rates of Campbell and Wang [16] plus fluorescence and Coster-Kronig yields of Campbell [17], corrected for multiple ionizations as prescribed by Eqs. (8)–(10), is the optimal selection of atomic parameters modified in the best possible manner for multiple ionization. However, we submit that—given the availability of 3 sufficiently well-resolved $L\gamma$ subpeaks—the choice of atomic parameters corrected for multiple-ionization should be routinely scrutinized by *all* 6 methods of data extraction.

We found no carbon-induced *L*-subshell cross sections in the literature for comparison with our Re data. The *L*-subshell ionization cross sections for 4.8–21.6-MeV carbon on Pt and Au by Semaniak *et al.* [15] were already corrected for effects of multiple ionization; unfortunately, the measured x-ray production cross sections were not given in Ref. [15]. Table IV lists other cross sections found in the literature for gold, after correction for multiple ionization with Eqs. (8)–(10). With their choice of atomic parameters from Krause [39] and Scofield [40], we converted the *L*-subshell ionization cross sections of Sarkadi and Mukoyama [12] back to their x-ray peak cross sections, and then extracted ionization cross sections with the atomic parameters of Table II corrected for multiple ionization. Without identifying the charge state of their carbon ions, Malhi and Gray measured only $\{L\alpha, L\gamma_1, L\gamma_{23}\}$ x-ray production cross sections [13]. We assumed that these ions were in an equilibrated charge state as given by Eq. (3) of Ref. [27], and using our fourth method extracted *L*-subshell ionization cross sections from $\{L\alpha, L\gamma_1, L\gamma_{23}\}$ x-ray production cross sections as listed in Table IV. Also shown in this table are ionization cross sections obtained from x-ray production cross sections of Bhattacharya *et al.* [14] by averaging the results of the same six methods that were utilized in the analysis of our data.

III. COMPARISON WITH THEORIES OF *L*-SUBSHELL IONIZATION

In the first Born approximation the direct ionization to the target continuum is calculated in the plane-wave Born approximation [6] and electron capture is calculated with the OBK formulas of Nikolaev [7]. According to the standard ECPSSR theory [8,9] the contribution of electron capture to ionization increases with increasing projectile energy but is still practically negligible (less than 1% in the energy range of our data for C^{3+} on Re, Pt, and Au, and less than 3% for the highest carbon energy datum at 36 MeV [13]). The ECPSSR theory [8,9] is an improvement over the first Born approximation. It generally yields very good results for L_3 ionization, and for *L*-shell ionization when total *L*-shell ionization is dominated by the L_3 contribution. The standard ECPSSR theory tends to, respectively, generally overestimate and definitely underestimate L_1 and L_2 cross sections.

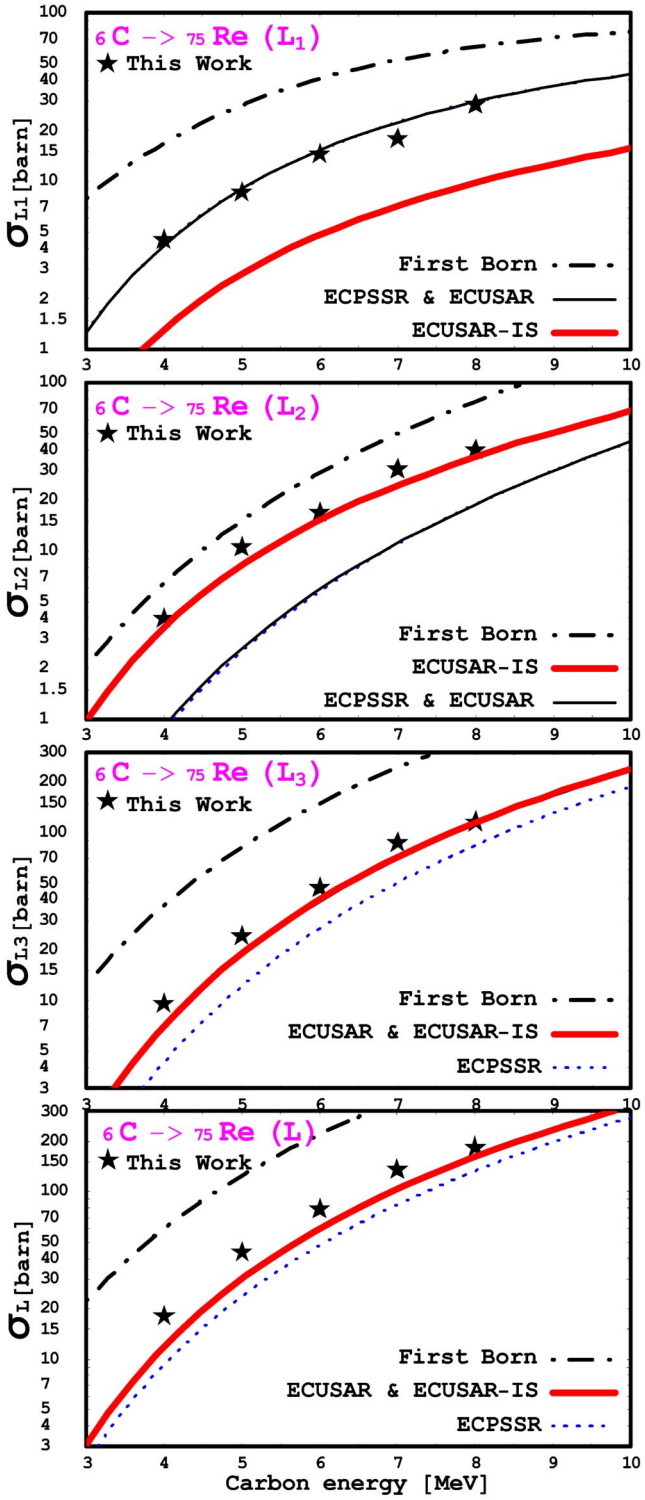

FIG. 2. *L*-subshell and *L*-shell ionization of rhenium by carbon ions compared with the first Born [6,7] (dot-dashed), ECPSSR [8,9] (dashed) and its modifications: ECUSAR (thin solid) for the united and separated atom (USA), Eq. (13), and ECUSAR-IS (thick solid) for the normalized intrashell (IS) coupling, Eq. (14) effects. For L_1 and L_2 subshells, the standard PSS approach and USA treatment of the binding effect yield essentially identical results in the displayed energy range.

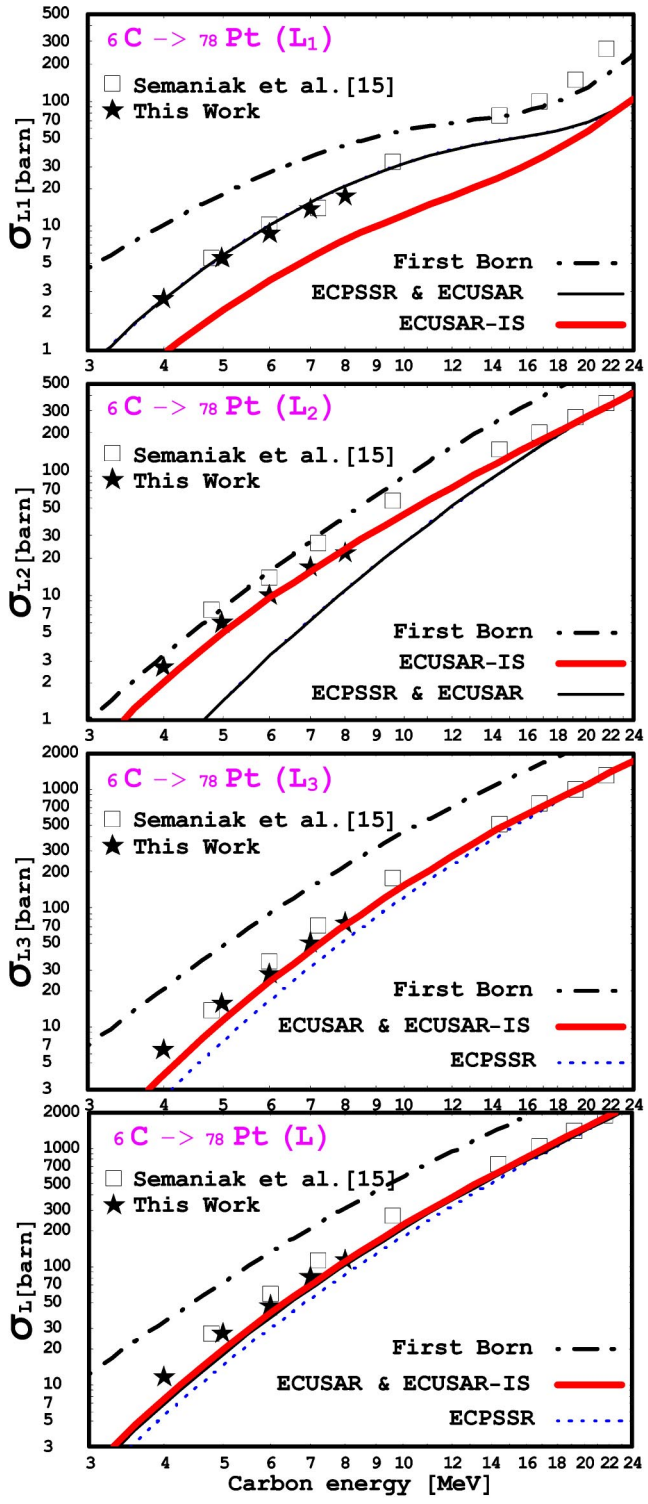

FIG. 3. As Fig. 2 for ionization of platinum by carbon ions.

Figures 2–4 show comparison of the extracted *L*-subshell ionization cross sections with the first Born and ECPSSR theories as well as the standard ECPSSR modified (a) with a united and separated atom (USA) treatment and (b) for intrashell (IS) couplings in the *L* shell.

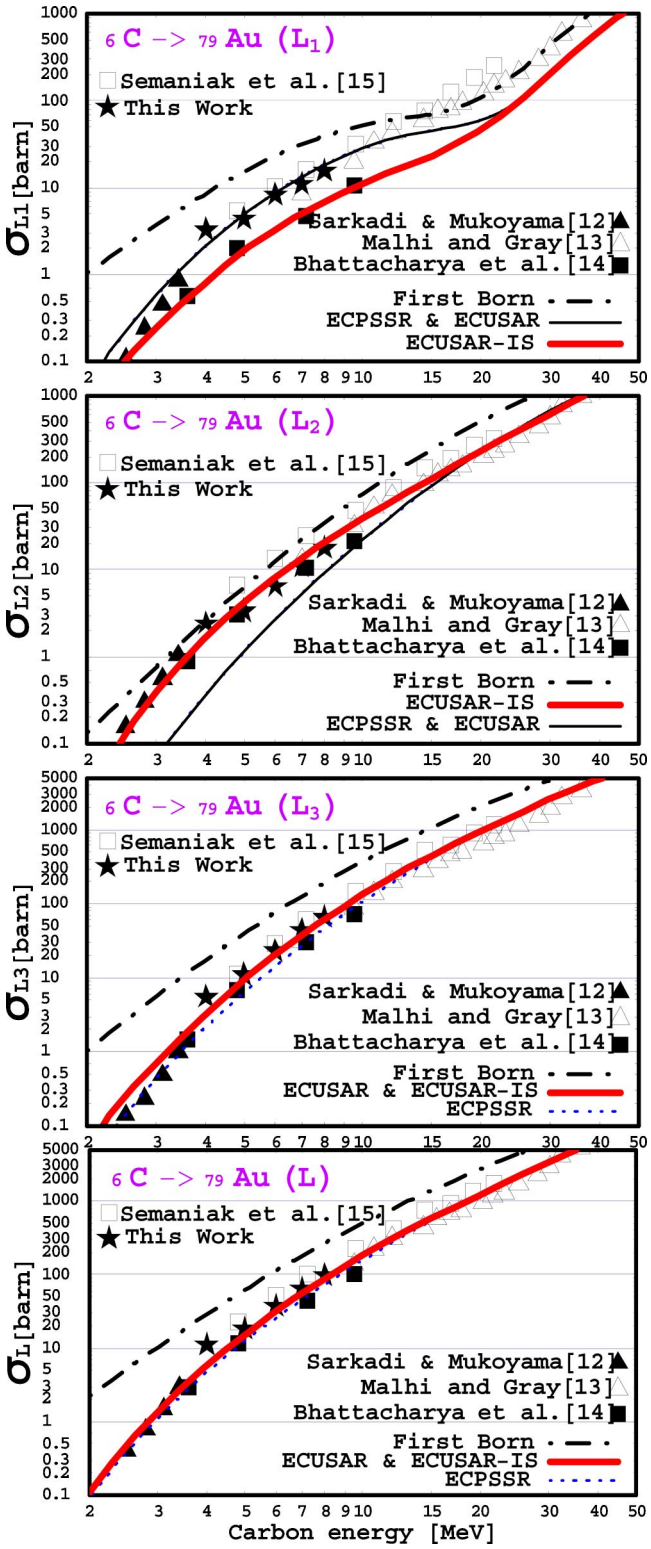

FIG. 4. As Fig. 2 for ionization of gold by carbon ions.

A. ECUSAR theory

In the standard ECPSSR, the binding energy of an inner-shell $S=K,L_1,\ldots$ electron is increased to an eigenenergy of the perturbed stationary state (PSS) of a separated atom (SA) so that θ_S, the observed binding energy divided by $\frac{1}{2}(Z_{2S}/n)^2$, changes to $\zeta_S\theta_S$, where

$$\zeta_S = 1 + (2Z_1/Z_{2S}\theta_S)[g_S(\xi_S) - h_S(\xi_S)]. \tag{11}$$

When $v_1 \ll v_{2S}=Z_{2S}/n$ in the very slow collision limit, $\xi_S = 2v_1/v_{2S}\theta_S \to 0$, $h_S(\xi_S)=0$ and $g_S(\xi_S)\to 1$ so that $\zeta_S \to 1 + (2Z_1/Z_{2S}\theta_S)$, while it should have been

$$\zeta_S^{\mathrm{UA}} = (1 + Z_1/Z_{2S})^2\theta_S^{\mathrm{UA}}/\theta_S \tag{12}$$

to match the binding energy of the united atom (UA), $\frac{1}{2}(Z_1+Z_{2S})^2\ \theta_S{}^{\mathrm{UA}}/n^2$. Following Vigilante *et al.* [41], various schemes have been suggested to combine the UA and SA treatments. In the ECUSAR theory, the united and separated atom (USA) functions are derived and valid in the complementary collision regimes of slow and intermediate to fast collisions, respectively, and smoothly joined with a simple formula [10]

$$\zeta_S^{\mathrm{USA}} = \zeta_S^{\mathrm{UA}} \text{ of Eq. (12) when } \zeta_S \geqslant \zeta_S^{\mathrm{UA}} \text{ and} \tag{13}$$

$$\zeta_S \text{ of Eq. (11) when } \zeta_S \leqslant \zeta_S^{\mathrm{UA}},$$

which replaces ζ_S that was derived in the separated atom PSS approach of the ECPSSR theory.

In the energy range of the data shown in Figs. 2–4, ECUSAR is identical with ECPSSR for L_1 and—with the exception of rhenium where it rises with decreasing energy to only 7% above ECPSSR at 4 MeV—for L_2. For L_3, the USA treatment of the binding effect is significant: the ECUSAR rises above the ECPSSR by as much as 70% at the lowest energy of 2.5 MeV in gold.

B. ECUSAR-IS theory

As do the first Born [6] and semiclassical [42] approximations, the standard ECPSSR treats the ionization of L subshells as mutually independent processes, neglecting intrashell (IS) coupling among these subshells. Progressing from a simple two-step model [43], second-order Born approximation [44], to coupled-states calculations [45], Sarkadi and Mukoyama developed means of accounting for the intrashell transitions. Coupled-state calculation of L-subshell ionization probabilities as a function of impact parameter by Legrand *et al.* [46] revealed the importance and systematics of the IS effect. While the IS transitions had practically no influence on L_3-subshell ionization, at small impact parameters L_2-subshell ionization was particularly strongly enhanced and the probability for L_1 ionization was depressed. As the contribution to ionization cross sections at these small parameters increases with decreasing projectile velocity, so is the role of the IS effect in determination of ionization cross sections and the manner in which they are altered. Indeed, the IS transitions practically had no effect on the L_3 cross section, and reckoning for the IS effects led to substantial improvement in agreement between the theory and the data for L_2 as contrasted with an underestimation of experimental L_1 ionization cross sections [47]. Due to simplifying assumptions, the coupled-state calculations of Sarkadi and Mukoyama [43–46] underestimated subshell cross sections and so their sum was less than the total L-shell ionization evaluated without the IS effect. Pajek *et al.* [11] rectified this problem by normalizing IS factors such that they merely

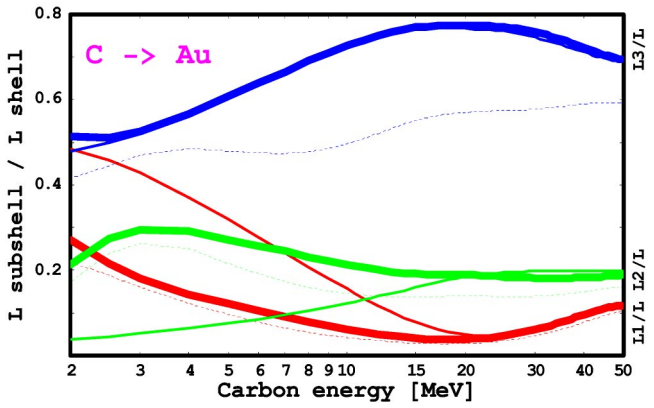

FIG. 5. Contributions of L-subshell ionization to L-shell ionization of gold by carbon ions according to the ECPSSR (dashed curves), ECUSAR (solid curves), and ECUSAR-IS (thick solid curves) theories.

redistributed collisionally-induced L-subshell vacancies without affecting the total L-shell cross section. We have normalized the IS factors, c_i, calculated for our collision systems by Sarkadi [48] so that $\Sigma\sigma_{Li}^{\text{ECUSAR-IS}}=\Sigma\sigma_{Li}^{\text{ECUSAR}}$. Hence

$$\sigma_{Li}^{\text{ECUSAR-IS}}=c_i\sigma_{Li}^{\text{ECUSAR}}\sum\sigma_{Li}^{\text{ECUSAR}}/\sum c_i\sigma_{Li}^{\text{ECUSAR}}. \tag{14}$$

Figure 5 shows that the fractional contribution of L_3-subshell ionization to total L-shell ionization is practically the same in the ECUSAR (solid curve) and ECUSAR-IS (thick solid curve) theories; according to the standard ECPSSR (dashed curve) this contribution is significantly less than in either of its modifications. As depicted in Figs. 2–4, predictions of these theories for L_1 and L_2 bifurcate with decreasing energy of carbon ions: the inclusion of the IS effect produces significant decrease of the L_1 and comparably significant enhancement in the L_2 contributions to the L-shell ionization. For L_2, the ECUSAR-IS is clearly superior to ECUSAR, and on the average is within 25% from the present work and each reference other than Ref. [15] whose data ECUSAR-IS underestimates by as much as nearly a factor of 2 at the lowest carbon energies. For L_3, both theories compare equally well (with the exception of Ref. [15] and on the average within 30%) with the data extracted from our measurements in all targets as well as—when averaged with other data [12–14]—in gold. As seen in Figs. 2–4, to the extent that L_3 subshell dominates the total L-shell ionization cross sections (see Fig. 5), such cross sections are also in very good agreement with the data taken as the sum of the extracted L-subshell ionization cross sections.

In the calculations of the total L-shell ionization cross sections, by definition, the ECUSAR and ECUSAR-IS are identical. This is not exactly the outcome after subshell ionization cross sections $\{\sigma_{L_1},\sigma_{L_2},\sigma_{L_3}\}$ are multiplied by the effective fluorescence yields, $\{\omega_1+f_{12}\omega_2+(f_{12}f_{23}+f_{13})\omega_3,\omega_2+f_{23}\omega_3,\omega_3\}$, and summed up to obtain the L-x-ray production cross section for comparison with the data in cases when the L-subshell x-ray production cross sections were not reported. However, the differences between the conversion of the ECUSAR and ECUSAR-IS ionization to x-ray cross sections are minute because the IS coupling does not affect the dominating contribution from the L_3 subshell and, outside of very low energy regime, the troublesome L_1 contributes typically no more than 10% to L-shell ionization (see Fig. 5). L-x-ray production cross sections calculated with ECUSAR are only a few percent smaller than if they are evaluated with the ECUSAR-IS L-subshell ionization cross sections. Excellent agreement of either of these theories with L_3 subshell ionization data ensures that one gets equally good agreement with the L-x-ray production measurements (see Figs. 2–4). For example, within the range of 10% experimental uncertainties, the calculated 760 b for L-x-ray production in gold by 25-MeV C^{4+} ions compares very well with 670 b measured by Andrews *et al.* [49].

L_1 subshell presents the greatest challenge. As seen in Figs. 2–4 and amplified in the ratio plots in Figs. 6–8, our data are in remarkably close agreement with the predictions of the ECPSSR and ECUSAR theories, while they are, by as much as factors 2 to 3, above the ECUSAR-IS predictions. Although Semaniak *et al.* [15] converted their x-ray production cross sections with a different set of atomic parameters corrected for multiple ionization in a different manner—that they themselves have since abandoned [23]—their L_1 ionization cross sections as well those from Malhi and Gray [13] are almost indistinguishable from our data and the ECPSSR or ECUSAR in the 4–8 MeV range. On the other hand, the lowest energy data of Sarkadi and Mukoyama [12] and measurements of Bhattacharya *et al.* [14] in the energy range of our experiment fall by a factor of 2 below our data and remarkably well along the ECUSAR-IS curve. Perhaps even more perplexing are two facts: (a) above 2 MeV/u especially data from Ref. [13] fall along the prediction of the first Born approximation, and (b) the data of Refs. [13,15] do not exhibit a knee in the 0.5–2 MeV/u range—which due the nodal character of the 2*s* state wave function does appear at these velocities in ionization by protons (see, for example, Fig. 9 in Ref. [36]) and heavier ions [50] or shows up as a minimum in $\sigma_{L_1}/\sigma_{L_2}$ ratios measured with protons and heavier ions [51]. Since Gray and his earlier co-workers saw no discernable plateau in $L\gamma_{23}$ x-ray production by oxygen ions in the same 0.5–2 MeV/u range on six other elements [19], Shingal *et al.* [52] attempted to explain these facts with target-centered coupled channel calculations by fully stripped heavy ions. In a sequel to [13,52] that criticizes the ECPSSR success as fallacious, Malhi and Gray [53] mention that the target thickness exceeded the vacancy equilibration distances—which justifies our assumption that q in Eq. (10) should be an equilibrated charge for their data—and state that their analysis was sound because the L-subshell ionization was dominated by direct ionization, which confirms that the incident ions were not fully stripped. Even if carbon was fully stripped, a 4% contribution of electron capture at 3 MeV/u would not have bridged the gap between the identical predictions of the ECPSSR theory and its modifications and the Malhi and Gray data. Moreover, this 4% contribution is calculated for electron capture from a single target atom. Based on a recent study of the influence of the target density

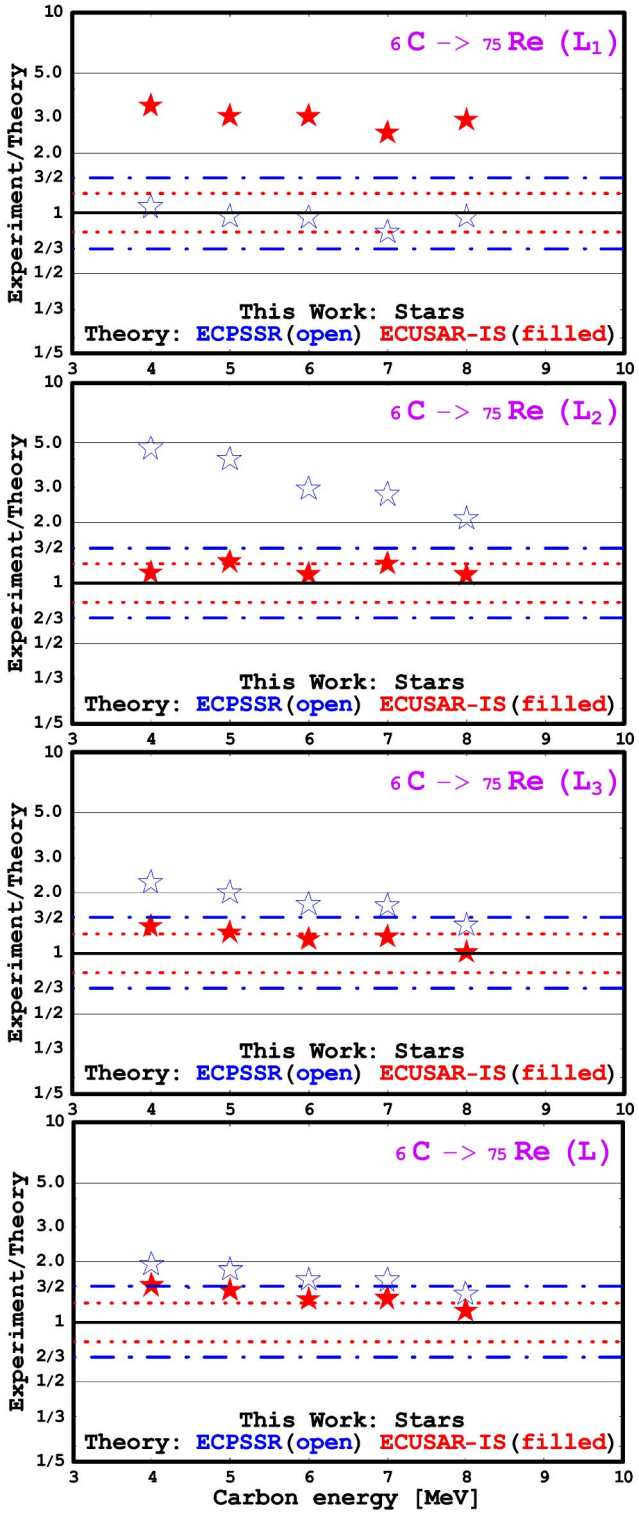

FIG. 6. Ratio of the data to predictions of the ECPSSR (open symbols) and ECUSAR-IS (filled symbols) theories for ionization of rhenium by carbon ions.

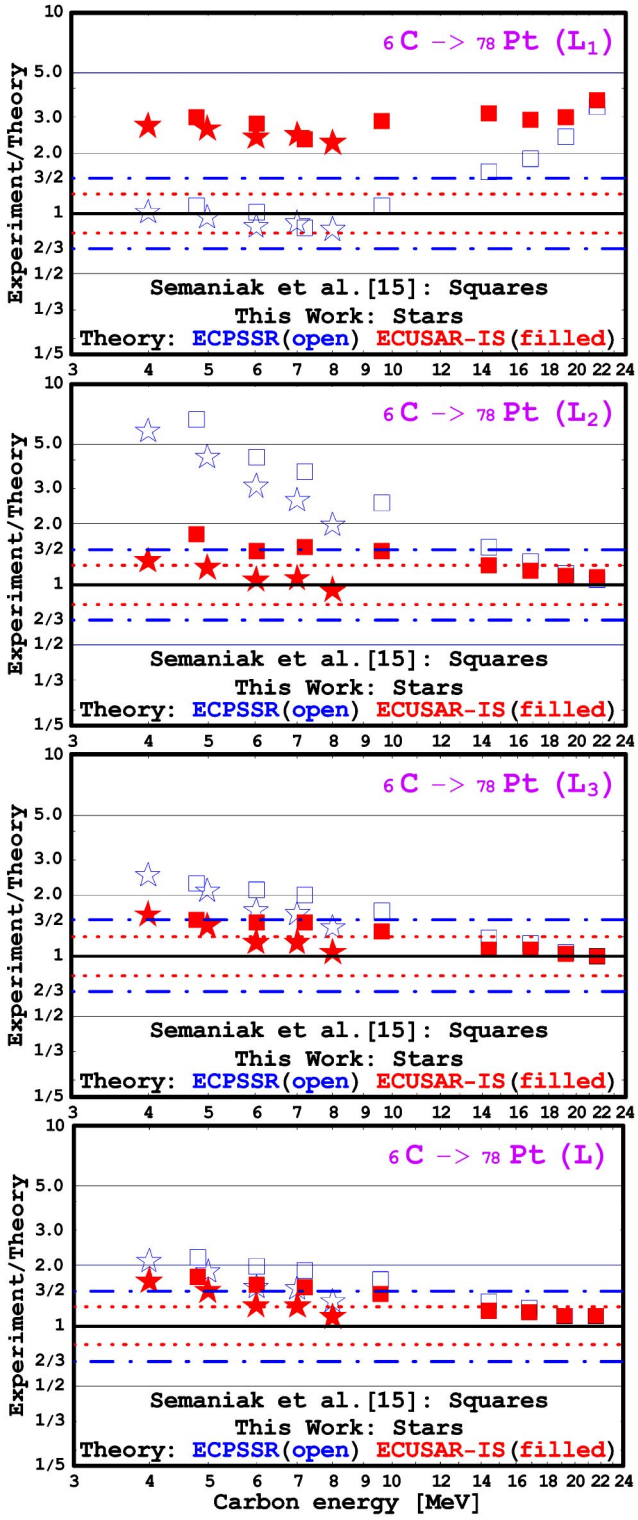

FIG. 7. Ratio of the data to predictions of the ECPSSR (open symbols) and ECUSAR-IS (filled symbols) theories for ionization of platinum by carbon ions.

on the electron capture process by Shevelko *et al.* [54], at 3 MeV/u (see Fig. 8 in Ref. [54]) the contribution of electron capture in a solid target is an order of magnitude smaller than 4%.

Except for the data of Ref. [14] that are in remarkably excellent agreement with the ECUSAR-IS results, on the average the ECUSAR-IS theory underestimates the data by 110%, 150%, and 200% for L_1-subshell ionization in Au, Pt,

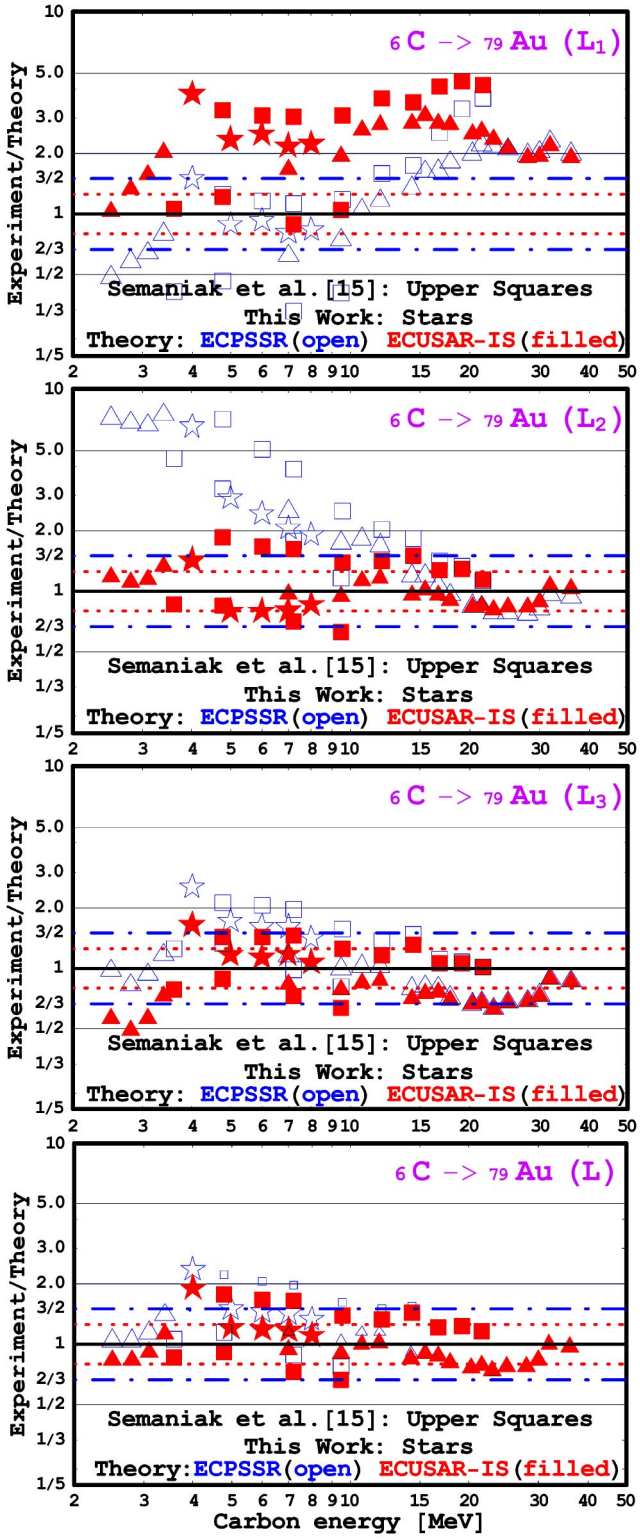

FIG. 8. Ratio of the data to predictions of the ECPSSR (open symbols) and ECUSAR-IS (filled symbols) theories for ionization of gold by carbon ions. The triangles at C energy <3.5 MeV represent the ratios of cross sections measured by Sarkadi and Mukoyama [12], the triangles at C energy >6 MeV correspond to the data of Malhi and Gray [13], and lower squares are based on the data of Bhattacharya *et al.* [14].

and Re. Perhaps, when more data become available for Pt and Re, this theory will emerge—as it does for Au—as exceeding experiment by about a factor of 2 for all targets. We cannot eliminate this large factor by an additional factor of 2 via a further adjustment of atomic parameters. The critical changes of ω_1^o and f_{13}^o have been made by Eqs. (8)–(10); these changes already modified ω_1^o and f_{13}^o by large factors—to a degree that coincides with the alteration of f_{13}^o and value of ω_1 by Banaś *et al.* due to closing of Coster-Kronig transitions in gold atoms multiply ionized by oxygen ions [55]. Jitschin *et al.* [37] noted two decades ago that as a consequence of this closing "the large Coster-Kronig rate f_{13}^o may be drastically reduced and the fluorescence yield ω_1^o increased by a factor of two." Equation (9), in perfect conformity with Fig. 2 of Ref. [55], indeed reduces f_{13}^o by this factor. Although Eq. (8) enhances $\omega_1^o=0.13$ only 50–20 % in the 4–8 MeV range of C→Au data, our values of ω_1 are comparable to those that were shown in Fig. 1 of Ref. [55] for O→Au. The final figure in Ref. [11] exhibits deviations by almost a factor of 2 and above for *all* L subshells, while we see it only for the L_1 subshell. While our data for L_1 are greater by factors of 2 to 3 than the predictions of the ECUSAR-IS theory, the L_1-subshell ionization data with carbon on gold [15] exceed these predictions by factors of 3 to 5.

In the work of Pajek *et al.* [11,15,55], multiple ionizations have relatively very small influence on ω_2^o, ω_3^o, f_{12}^o, and f_{23}^o with ω_2, f_{12}, and f_{23} being practically independent of the projectile energy (see Figs. 1 and 2 in Ref. [55]). These findings are consistent with the fact that multiple ionization has slight effect on these parameters in the L_2- and L_3-subshell ionization by light ions [56] but may not be true for ionization by heavy ions. In our calculations, changes in ω_2^o, ω_2^o, f_{12}^o, and f_{23}^o are made in the same degree as for ω_1^o and f_{13}^o, and they subside with the increasing projectile energy. Consequently, while our ratios of experiment to theory stay, within experimental uncertainties, close to 1 at *all* energies for the L_2 and L_3 subshells (see Figs. 6–8), Fig. 16 of Ref. [11] shows deviations by a factor of nearly 2; they gradually disappear only at higher energies where multiple ionizations are of diminishing importance as the probability of outer shell ionization P given by Eq. (10) decreases with increasing projectile energy to the small values which Pajek *et al.* have inferred from their procedures. The same trend of vanishing importance of multiple ionization for L_2 and L_3 subshells at higher energies would have been seen in Fig. 7 of Ref. [15] if the theoretical calculations for L_2 were corrected for the normalized IS effect which does not affect the L_3 calculations. Although the present manner of accounting for effects of multiple ionization and intrashell coupling brought the modified ECPSSR theory into a better overall agreement with the data than procedures of Ref. [11], we shall not conclude that "a substantial improvement is achieved, in particular for the L_1 subshell" as asserted in the recent work of Pajek *et al.* [11].

IV. WAVE-FUNCTION CORRECTION: W-ECUSAR-IS THEORY

The ECPSSR cross sections are cast in terms of the PWBA cross sections evaluated with the screened hydrogenic

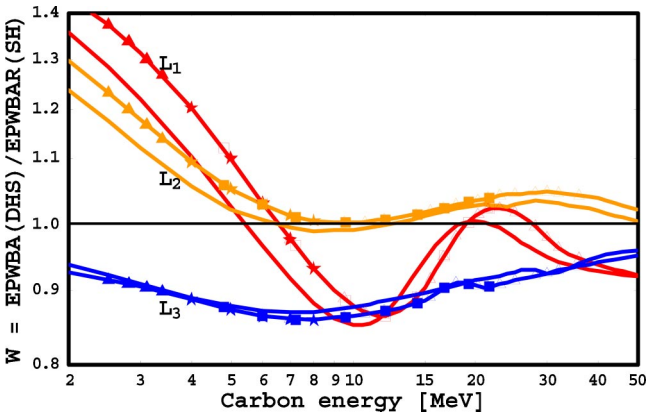

FIG. 9. Wave-function correction factor defined as the ratio of subshell ionization cross sections calculated by Chen and Crasemann in the EPWBA with the Dirac-Hartree-Slater wave functions [57] to the EPWBA evaluated with the screened hydrogenic wave functions corrected for the relativistic effect as in the ECPSSR [8]. The letter E signifies that both calculations were done with the exact limits on the minimum and maximum momentum transfers. These ratios were evaluated with the EPWBA(DHS) cross sections tabulated for 0.15–5 MeV protons on $_{75}$Re and $_{79}$Au [57], and scaled for carbon ions of the same velocity. The symbols on the Au curves are placed at the energies of our data and those of Refs. [12–15]. No symbols were placed on the $_{75}$Re curves to distinguish them from the gold curves, and the $_{78}$Pt curves, which are very close to the $_{79}$Au curves, are not displayed in this figure.

(SH) wave functions. To assess the role of wave functions we define a W_i factor

$$W = \sigma_{Li}^{\mathrm{EPWBA(DHS)}}/\sigma_{Li}^{\mathrm{EPWBAR(SH)}}, \tag{15}$$

where E signifies that the PWBA cross sections were calculated with the exact momentum transfer limits. $\sigma_{Li}^{\mathrm{EPWBA(DHS)}}$ is taken from Chen and Crasemann [57] who calculated it using the Dirac-Hartree-Slater wave functions; $\sigma_{Li}^{\mathrm{EPWBAR(SH)}}$ is evaluated with nonrelativistic screened hydrogenic wave functions and with accounting for the relativistic effect as formulated in the ECPSSR theory [8]. The ECPSSR and its modifications are simply multiplied by this factor to obtain cross sections based on the DHS wave functions. As seen in Fig. 9, the W factor lowers L_3 cross sections by about 10% and raises L_2 cross sections by about 20% for the data at the lowest energies. For L_1, this factor falls about 10% at 1 MeV/u and rises about 35% above 1 at the lowest energies.

Overall, the changes due to better wave functions are of lesser importance than due to the replacement of the ECPSSR with its ECUSAR modification for L_3 ionization, and definitely small compared to the IS effect in L_1 and L_2 ionization. From this perspective the total L-shell ionization, to which L_2 and L_3 make an 80–90 % contribution, is not very sensitive to the choice of wave functions.

V. CONCLUSIONS

We have compared averages of the ratios of ionization cross sections—extracted from the data from our present and other work [12–14]—to the predictions of ECUSAR-IS theory versus the averaged ratios of these data to the results of the W-ECUSAR-IS theory. For each subshell and total L shell, Table V shows the percentage difference of these averaged ratios from the ideal ratio of 1; the first row obtains when ECUSAR-IS is used and the second row follows when W-ECUSAR-IS is employed. The differences between the data and these two theories are emphasized in the bold print for the theory that gives better results. When these percentage differences are large, the ECUSAR-IS based on screened hydrogenic wave functions appears to be generally slightly better than the W-ECUSAR-IS. When these percentage differences become comparable with 10–20 % uncertainties in the experimental cross sections, no distinction can be made between the ECUSAR-IS and W-ECUSAR-IS.

TABLE V. Percentage difference from the ideal ratio of 1 for ratios of experimental L-subshell ionization cross sections from Refs. [12–14] and this work to the theoretical L-subshell ionization cross sections according to the ECUSAR-IS (first row) and W-ECUSAR-IS (second row).

L_1	L_2	L_3	L	
Sarkadi and Mukoyama (1980)		Ref. [12]		C→Au
+49	**+19**	**−41**	−7	
+95	+41	−47	**+5**	
Malhi and Gray (1991)		Ref. [13]		C→Au
+137	−5	**+24**	−19	
+126	**+2**	−32	**−13**	
Bhattacharya *et al.* (1994)		Ref. [14]		C→Au
+6	−24	**−24**	**−21**	
+12	**−19**	−34	+24	
This work				C→Au
+164	−6	+24	+32	
+182	**−2**	**+8**	**+26**	
Data from all the above references				C→Au
+111	**−4**	**−18**	−9	
+116	+4	−27	**−5**	
This work				C→Pt
+150	**+12**	+28	+36	
+159	+16	**+11**	**+28**	
This work				C→Re
+199	**+17**	+20	+34	
+196	+19	**+6**	**+25**	

The ECUSAR-IS theory is in very good, on the average 30%, agreement with our data for L_2 and L_3 ionization of all three targets. Except for the data from Refs. [12,15], this is also true for the other data [13,14]. On the average, the gold data for L_2 from other references are greater in Refs. [12,15] and smaller in Refs. [13,14] and our work than the predictions of the ECUSAR-IS theory while—contrary to our data—the gold data for L_3 of all other references are overestimated by this theory. However, as the deviations between the data and the ECUSAR-IS theory are comparable to the uncertainties in these data and they fall on both sides of the ideal ratio of 1, there is no systematic and significant differ-

ence between this theory and experimental ionization for the L_2 and L_3 subshells.

A long-standing discrepancy observed for the L_1 subshell remains unresolved, aggravated by the problem of large scatter of the experimental data demonstrated here for gold ionization by carbon ions (see Table V plus Figs. 4 and 8), and recognized before for protons [5,10]. It could be that the very analysis of the measured x-ray spectra is at fault. Papp and Campbell [58] demonstrated that even for proton-induced x-ray spectra the common practice of neglecting the natural line shapes and related issue of what constitutes the background produce systematic errors, especially for x rays originating from the L_1 and L_2 subshells, and reiterated that the line shape effect is expected to be even more important in the case of multiply ionized atoms. In particular, with the larger L_2 than L_1 contribution from the spread of the Lorentzian wings under small $L\gamma$ subpeaks, the extracted L_1-subshell ionization cross sections could have been significantly overestimated because some fraction of them should have been attributed to L_2—the fraction that was undetected by the conventional Gaussian fits. In fact, Table III shows that the $L\gamma_1$ peak obtained by a Gaussian fit gives systematically larger L_1 ionization cross sections than the other five Gaussian peaks. The more accurate, smaller $L\gamma_1$ would lead via the Datz technique to a smaller $L\gamma_{23}$ and, hence, smaller L_1. Likewise or maybe more critically, the smallest peak $L\gamma_{4,4}$ that at present is connected solely with L_1 by Eq. (7) could have been substantially a part of the Lorentzian wings from large L_2 and L_3 contributions to the analyzed spectrum. All these scenarios, which are particularly realistic when peaks are shifted to higher energies and widened by a high degree of multiple ionization, could occur synergistically and explain why L_1 subshell ionization is systematically overestimated by the conventional spectra analysis.

ACKNOWLEDGMENTS

We are grateful to Ian Campbell for valuable comments on S_{pi}, and to László Sarkadi for calculation of the intrashell coupling factors c_i. One of us (S.B.R.) acknowledges financial support provided by the Inter University Consortium for DAE facilities at the Kolkata center, India, and A.K. Sinha for his valuable suggestions and encouragement. We also highly appreciate the technical assistance rendered by the staff of the pelletron accelerator facility at the Institute of Physics, Bhubaneswar.

[1] H. Paul, Nucl. Instrum. Methods Phys. Res. B **3**, 3 (1984).
[2] H. Paul and J. Sacher, At. Data Nucl. Data Tables **42**, 105 (1989).
[3] G. Lapicki, J. Phys. Chem. Ref. Data **18**, 111 (1989).
[4] H. Paul and O. Bolik, At. Data Nucl. Data Tables **54**, 75 (1993).
[5] I. Orlic, C.H. Snow, and S.M. Tang, At. Data Nucl. Data Tables **56**, 159 (1994).
[6] B.-H. Choi, E. Merzbacher, and G.S. Khandelwal, At. Data **5**, 291 (1973).
[7] V.S. Nikolaev, Zh. Eksp. Teor. Fiz. **51**, 1263 (1966); [Sov. Phys. JETP **24**, 847 (1967)].
[8] W. Brandt and G. Lapicki, Phys. Rev. A **23**, 1717 (1981).
[9] G. Lapicki and F.D. McDaniel, Phys. Rev. A **22**, 1896 (1980).
[10] G. Lapicki, Nucl. Instrum. Methods Phys. Res. B **189**, 8 (2002).
[11] M. Pajek, D. Banaś, J. Semaniak, J. Braziewicz, U. Majewska, S. Chojnacki, T. Czyżewski, I. Fijał, M. Jaskóła, A. Glombik, W. Kretschmer, D. Trautmann, G. Lapicki, and T. Mukoyama, Phys. Rev. A **68**, 022705 (2003).
[12] L. Sarkadi and T. Mukoyama, J. Phys. B **13**, 2255 (1980).
[13] N.B. Malhi and T.J. Gray, Phys. Rev. A **44**, 7199 (1991).
[14] D. Bhattacharya, M. Sarkar, M.B. Chatterjee, P. Sen, G. Kuri, D.P. Mahapatra, and G. Lapicki, Phys. Rev. A **49**, 4616 (1994).
[15] J. Semaniak, J. Braziewicz, M. Pajek, T. Czyżewski, L. Głowacka, M. Jaskóła, M. Haller, R. Karschnik, W. Kretschmer, Z. Halabuka, and D. Trautmann, Phys. Rev. A **52**, 1125 (1995).
[16] J.L. Campbell and J.-X. Wang, At. Data Nucl. Data Tables **43**, 281 (1989).
[17] J.L. Campbell, At. Data Nucl. Data Tables **85**, 291 (2003).
[18] D.K. Olsen, C.F. Moore, and P. Richard, Phys. Rev. A **7**, 1244 (1973).
[19] G.H. Pepper, R.D. Lear, T.J. Gray, R.P. Chatuverdi, and C.F. Moore, Phys. Rev. A **12**, 1237 (1975); W. Uchai, G. Lapicki, W.T. Milner, S. Raman, P.V. Rao, and C.R. Vane, J. Phys. B **18**, L389 (1985).
[20] C. Berinde, C. Ciortea, A. Enulescu, D. Fluerașu, G. Hock, I. Piticu, L. Sarkadi, B. Sulik, and V. Zoran, J. Phys. B **20**, L481 (1987).
[21] F. P. Larkins, J. Phys. B **4**, L29 (1971).
[22] Y. Ramakrishna, K.R. Rao, G.J.N. Raju, K.B. Rao, V.S. Rao, P. Venkateswarlu, and S.B. Reddy, Pramana **59**, 685 (2002).
[23] M. Pajek, D. Banaś, J. Braziewicz, U. Majewska, J. Semaniak, T. Czyżewski, M. Jaskóła, W. Kretschmer, T. Mukoyama, D. Trautmann, and G. Lapicki, in *Application of Accelerators in Research and Industry*, edited by J.L. Duggan and I.L. Morgan, AIP Conf. Proc. No. 475 (AIP, Woodbury, NY, 1999), p. 32. See also D. Banaś, M. Pajek, J. Semaniak, J. Braziewicz, A. Kubala-Kukuś, U. Majewska, T. Czyżewski, M. Jaskóła, W. Kretschmer, T. Mukoyama, and D. Trautmann, Nucl. Instrum. Methods Phys. Res. B **195**, 233 (2002) and Refs. [7–9] therein.
[24] B. Sulik, G. Hock, and D. Berényi, J. Phys. B **17**, 3269 (1984).
[25] G. Lapicki, R. Mehta, J.L. Duggan, P.M. Kocur, J.L. Price, and F.D. McDaniel, Phys. Rev. A **34**, 3813 (1986).
[26] R. Mehta, H.L. Sun, D.K. Marble, J.L. Duggan, F.D. McDaniel, and G. Lapicki, J. Phys. B **28**, 1187 (1995).
[27] G. Schiwietz and P.L. Grande, Nucl. Instrum. Methods Phys. Res. B **175/177**, 125 (2001).
[28] A. G. Kochur and V. L. Sukhorukov, J. Phys. B **29**, 3587 (1996).
[29] A. El-Shemi, Y. Lofty, and G. Zschornack, J. Phys. B **30**, 237

(1997).
[30] C. O. Reinhold, D. G. Arbó, J. Bűrgdorfer, B. Gravais, E. Lamour, D. Vernhet, and J. P. Rozet, J. Phys. B **33**, L111 (2000).
[31] H. O. Lutz, J. Stein, S. Datz, and C. D. Moak, Phys. Rev. Lett. **28**, 8 (1972).
[32] S. L. Sorensen, S. J. Schaphorst, S. B. Whitfield, B. Crasemann, and R. Carr, Phys. Rev. A **44**, 350 (1991).
[33] M. Lorenz and E. Hartmann, J. Phys. B **20**, 6195 (1987).
[34] D.D. Cohen, J. Phys. B **17**, 3913 (1984).
[35] Y.P. Singh, D. Mitra, L.C. Tribedi, and P.N. Tandon, Phys. Rev. A **63**, 012713 (2000).
[36] S. Datz, J.L. Duggan, L.C. Feldman, E. Laegsgaard, and J.U. Andersen, Phys. Rev. A **9**, 192 (1974).
[37] D.D. Cohen, J. Phys. B **18**, 3607 (1985).
[38] W. Jitschin, R. Hippler, K. Finck, R. Schuch, and H. O. Lutz, J. Phys. B **16**, 4405 (1983).
[39] M.O. Krause, J. Phys. Chem. Ref. Data **8**, 307 (1979).
[40] J.H. Scofield, At. Data Nucl. Data Tables **14**, 121 (1974).
[41] M. Vigilante, P. Cuzzorcea, N. De Cesare, F. Murolo, E. Perillo, and G. Spadacini, Nucl. Instrum. Methods Phys. Res. B **51**, 232 (1990).
[42] J. M. Hansteen and O.P. Mosebekk, Z. Phys. **234**, 281 (1970).
[43] L. Sarkadi and T. Mukoyama, J. Phys. B **14**, L225 (1980).
[44] L. Sarkadi and T. Mukoyama, Nucl. Instrum. Methods Phys. Res. B **4**, 286 (1984); L. Sarkadi, J. Phys. B **19**, 2319 (1986).
[45] L. Sarkadi, J. Phys. B **19**, L755 (1986); L. Sarkadi and T. Mukoyama, *ibid.* **20**, L559 (1987); J. Phys. B **23**, 3849 (1990).
[46] I.C. Legrand, V. Zoran, R. Dörner, H. Schmidt-Böcking, A. Berinde, D. Fluerasu, and C. Cioretea, J. Phys. B **28**, 189 (1992).
[47] M. Sarkar, D. Bhattacharya, M.B. Chatterjee, P. Sen, G. Kuri, D. P. Mahtapatra, and G. Lapicki, Nucl. Instrum. Methods Phys. Res. B **103**, 23 (1995).
[48] L. Sarkadi (private communication).
[49] M.C. Andrews, F.D. McDaniel, J.L. Duggan, P.D. Miller, P.L. Pepmiller, H.F. Krause, T.M. Rosseel, L.A. Rayburn, R. Mehta, and G. Lapicki, Phys. Rev. A **36**, 3699 (1987).
[50] B.B. Dhal, T. Nandi, and H.C. Padhi, Nucl. Instrum. Methods Phys. Res. B **101**, 327 (1995).
[51] T.K. Li, D.L. Clark, and G.W. Greenlees, Phys. Rev. Lett. **37**, 1209 (1976).
[52] R. Shingal, N.B. Malhi, and T.J. Gray, J. Phys. B **25**, 2055 (1992).
[53] T.J. Gray and N.B. Malhi, J. Phys. B **23**, 3849 (1996).
[54] V. P. Shevelko, O. Rosmej, H. Tawara, and I.Y. Tolstikhina, J. Phys. B **37**, 201 (2004).
[55] D. Banaś, J. Braziewicz, M. Czarnota, I. Fijał, M. Jaskóła, A. Korman, W. Kretschmer, M. Pajek, and J. Semaniak, Nucl. Instrum. Methods Phys. Res. B **205**, 130 (2003).
[56] E. Perillo, G. Spadaccini, M. Vigilante, P. Cuzzocrea, and N.D. De Cesare, J. Phys. B **20**, 1275 (1987).
[57] M.H. Chen and B. Crasemann, At. Data Nucl. Data Tables **33**, 217 (1985); **41**, 257 (1989).
[58] T. Papp and J.L. Campbell, Nucl. Instrum. Methods Phys. Res. B **114**, 225 (1996).